Evaluation of the vibrational modes of the human skull as it relates to bone-conducted sound

Margaret G. Wismer and William D. O'Brien
Bioacoustics Research Lab, University of Illinois Urbana-Champaign, Urbana, Illinois 61801

(Received 8 June 2010; revised 16 August 2010; accepted 27 August 2010)

Analytic and numerical models are used to study bone-conducted sound and how it relates to the vibrational modes of the human skull. The analytic model is based on the solution to the acoustic and elastic wave equations and the constraining boundary conditions for a fluid-filled elastic sphere. Both models predict that most of the acoustic energy of bone-conducted sound exists in the form of surface wave vibrations at the interface between two acoustic media rather than in the bone or cranial chamber. These surface waves have phase speeds much slower than the bulk sound speed for bone. The analytic model, based on spherical elastic shells, predicts a phase speed of 775 m/s and the first resonance frequency at 1500 Hz while the numerical solution yields approximate phase speeds of 450 m/s and provides a visual display of the surface waves and diffraction effects.
 [DOI: 10.1121/1.3493432]

PACS number(s): 43.40.Fz, 43.80.Jz, 43.66.Wv [DF] Pages: 2792–2797

I. INTRODUCTION

Bone-conducted sound, which is the acoustic pressure that reaches the inner ear by pathways other than the normal air-conducted path, is of interest for its' effect on noise induced hearing loss (NIHL) and for its potential for secure communication in noisy environments. For NIHL the detailed means by which bone-conducted sound affects the middle and inner ears is investigated in order to design better hearing protection devices (HPDs). The U.S. Air Force has funded a program to determine the precise mechanisms of bone-conducted sound in order to mitigate the damaging effects for their personnel working in extreme high noise environments, such as under aircraft.

A better understanding of the effects of bone-conducted sound can be acquired through the study of the transmission of plane waves impinging upon the head in an air background. For a first approximation of the human head as a fluid filled spherical shell with a radius of 12.5 cm, the range of *ka* values, for sound signals, is roughly 0.2 through 20. For low frequencies, *ka* less than 1, most of the sound energy will penetrate the skull and travel through the head relatively unimpeded. With increasing frequency sound propagating in and around the skull will induce diffraction effects, in the form of airborne waves, on the surface of the skull and vibrational motions within the skull structure. The nature of bone-conducted sound is not best described in terms of high frequency wave propagation for which rays approximate the signal and which travel along prescribed paths.

One clearly defined bone-conducted sound path is due to an incoming wave that is diffracted around the outside of the skull. This diffracted wave travels in air but creeps along the skull surface at a sound speed close to the sound speed of air. It is often referred to as a Stoneley wave. The acoustic energy transmitted to the interior of the skull will cause structures within the skull to vibrate and these vibrations will be mostly confined to the interface surfaces such as exist between skull and soft tissue, analogous to plate flexural modes. It therefore makes sense to conceptualize bone-conducted sound in terms of structure vibrational modes rather than in terms of clearly defined pathways. The study of bone-conducted sound in terms of the skull resonance frequencies has a fairly deep publication record.[1,2] These studies rely on the forced response of bone anchored transducers attached to cadaver heads.

The cited phase velocities for bone-conducted sound is often given in the range of 200–400 m/s.[1,3] In these studies it is assumed that the sound speed corresponds to the speed of sound through bony tissue rather than on the skull surface. This is usually found via the results from phase shifts or time delays between sound signals at the two opposing mastoids and is not consistent with the measured acoustic properties of human bone[4] for which sound speeds are reported to be on the order of 3000 m/s. Based on the elastic properties of bone,[5] the transverse, or shear, sound speed is also on the order 2000 m/s. This paper attempts to clarify the nature of bone-conducted sound and explain the difference between bone-conducted sound speed and the measured elastic and acoustic properties of bone. The bone-conducted sound speed is explained by the combined presence of the "creeping waves"[6,7] which creep along the surface of the skull at speeds close to the speed of sound in air and resonant Rayleigh surface waves within the bone structure.

A study to better understand the interaction between acoustic pressure and the human skull is being conducted using both analytic and numerical simulation methods. Though results from Håkansson[2] indicate that vibrational modes vary widely across skull sizes and shapes, a first order, modal, analytic solution is available for approximating the skull as a fluid-filled elastic spherical shell. Though bone is inherently anisotropic this property is not as relevant at acoustic frequencies and the effects of skull thickness and fluid loading can be estimated via the acoustic resonance scattering theory (RST).[8]

The numerical model consists of a finite element algorithm based on the acoustic wave equation. The algorithm

uses as input the CT scan of a human skull in order to assess and visualize the interaction of an acoustic sound field with the complex structure of the skull. The model has been verified with the analytic solution of the spherical shell and is used to investigate and visualize the effects of surface waves on ellipsoidal shells as they would be closer to the skull shape. The remainder of this paper is organized as follows: Sec. II discusses the analytic results of plane waves hitting spherical targets in terms of form factors and the RST, Sec. III concentrates on the numerical algorithm and how it is used to study some of near-field effects of diffraction, and Sec. IV discusses the results.

II. THEORETICAL BACKGROUND

The existence of circumferential resonant sound waves on the surface of cylinders and spheres are predicted by the modal solution for the scattered field derived by Anderson for fluid spheres and Faran for elastic ones. For an acoustic plane wave, of frequency ω, colliding with an infinitely long cylinder, the scattered pressure, at position r, is expressed by the multipole expansion

$$p_{sc} = \frac{1}{2}\sum_n (i)^n(1+\delta_{n0})H_n^{(1)}(kr)(S_n-1)cos(n\theta). \tag{1}$$

For a sphere the multipole expansion becomes

$$p_{sc} = \frac{1}{2}\sum_n (2n+1)(i)^n(S_n-1)h_n^{(1)}(kr)P_n(\cos\,\theta), \tag{2}$$

in which S_n is a scattering function which depends on object construction such as whether it is purely rigid, solid elastic, solid fluid or a shell. Note that there is an implicit $e^{-i\omega t}$, in these expressions, which, when combined with either the $cos(n\theta)$ term for the cylinder or the Legendre function $P_n(\cos\,\theta)$ of the sphere, result in surface wave terms of the form $e^{i(n\theta-\omega t)}$. The remainder of this section will focus on the scattering solution due to spheres though there is an extensive parallel development for cylinders. If the sphere is purely rigid such that the sound wave cannot penetrate then $S_n=S_n^r=-h_n^{(2)'}(x)/h_n^{(1)'}(x)$ in which $x=ka$, $k=\frac{\omega}{c_1}$, a is the sphere radius and c_1 is the sound speed in the background medium. It has been demonstrated, through the RST,[8] that the far-field pressure scattered from the scattering object depends directly on the deformation or vibration patterns of the object. For the general case, the scattering function is reformulated as

$$S_n - 1 = S_n^r - 1 + \frac{2jS_n^r s_n^r}{F_n^{-1}(x) - \Delta_n^r - js_n^r}, \tag{3}$$

in which $\Delta_n^r = real(z_n^{(1)})$, $s_n^r = imag(z_n^{(1)}(x))$ and $z_n^{(1)}(x) = xh_n^{(1)'}(x)/h_n^{(1)}(x)$. In this form, the scattering function is separated into two terms one of which is due to scattering from a rigid sphere and one of which is due to resonance effects from the sphere medium. The first term (S_n^r-1) predicts low frequency resonances in the form of circular waves which vibrate within the surrounding background. A detailed explanation of these effects is given by Überall.[6] The second term predicts surface interface waves both within the background and within the sphere. When an integer number of wavelengths of these waves match the circumferential distance around the sphere, resonance effects occur causing the sphere to vibrate. Note that this separation is most pertinent if the sphere is a very dense, stiff almost rigid material similar to the skull in an air background. For spheres which are relatively soft with respect to the background medium the scattering function can be expressed as the sum of a resonant term and a term due to diffraction from a pressure release boundary. This second form would apply to air bubbles in water. Vibrational resonance frequencies are determined by setting the denominator of the resonance term, of Eq. (3), equal to zero and solving for x. The mode number, n, is related to the number of wavelengths on the sphere surface.

The simplest case is when the sphere medium is a fluid for which

$$F_n = \frac{\rho_1}{\rho_2}x_2\frac{j_n'(x_2)}{j_n(x_2)}, \tag{4}$$

in which ρ refers to density and the subscripts 1 and 2 are the background and interior, respectively. The form factors, and associated scattering function, for a pure elastic sphere is given by Faran,[9] for fluid-loaded elastic shell by Gaunaurd[10] and for the fluid-loaded fluid shell by McNew.[11]

For spheres much smaller than the wavelength of the incoming pressure signal (or $ka \ll 1$) only the first term in the modal solution is required and no resonances exist. As ka becomes larger more modal terms are required to resolve the reflected signal and to identify resonant frequencies (or frequencies at which the scattered signal becomes theoretically infinite.) Because there is a fluid/solid interface (in this case the fluid is air) most of the energy is channeled into Stoneley surface waves, which exist mostly in the fluid background, or Rayleigh surface waves, which exist mostly in the solid. When the wavelength matches the circumference distance around the sphere, energy is trapped on the surface causing amplified vibrations. Relatively low resonance frequencies are more prevalent when the impedance mismatch between the target and background is small and more acoustic energy is able to penetrate the sphere. If the sphere is much denser and stiffer than the background, (as is the case for bone-conducted sound) then the resonance frequencies are pushed to higher values and the creeping diffracted waves are more prevalent. For the fluid-loaded elastic spherical shell some of the energy is trapped in standing waves on the shell analogous to Lamb waves in plates. The sound speed for these waves is determined from a complex dispersion relation which depends on frequency, shell thickness, and sound speed of fluid, shell and background material. Each mode number will have its own set of resonance frequencies for which modal vibrations exist on the sphere. The mode number predicts the number of wavelengths present on the sphere such that for mode, n,

$$\lambda = \frac{2\pi a}{n+\frac{1}{2}}. \tag{5}$$

For the resonance frequency, $(ka)_{nl}$, the wave speed is therefore

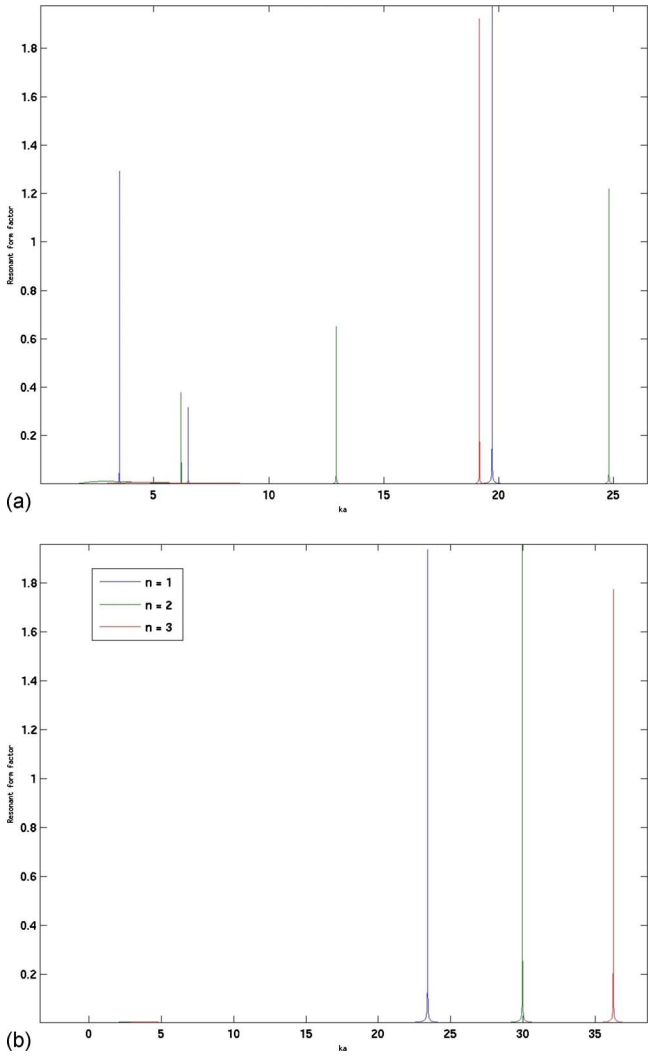

FIG. 1. (Color online) (a) Resonant form factor showing first three modes of a 25 cm diameter spherical *elastic* shell with thickness of 0.75 cm. (b) Resonant form factor showing first three modes of a 25 cm diameter spherical *fluid* shell with thickness of 0.75 cm.

$$c_p = \frac{(ka)_{nl}c}{n+\frac{1}{2}}. \tag{6}$$

Each mode will have multipole resonances for which the index l refers to the order resonance of the n^{th} mode. The longest dimension of a human skull is approximately 20–25 cm from front to back. The second term of Eq. (3) is plotted in Fig. 1. The resonance frequencies, for the first three modes, are shown in Fig. 1(a) for a 25 cm diameter elastic spherical shell with a shell thickness of 7.5 mm, the nominal thickness of a human skull. The shell has the elastic properties of bone with the interior having the acoustic properties of soft tissue and the exterior having the acoustic properties of air as given in Table I. The lowest resonance, which is in the, $n=1$ dipole mode, is around 1500 Hz which is slightly above the range of the lowest resonance given by Håkansson.[2] At this resonance $ka \approx 3.5$ corresponding to a phase speed of approximately 775 m/s. For comparison resonances for a fluid sphere in which the shell is assumed a fluid with a sound speed equivalent to the longitudinal speed of sound are shown in Fig. 1(b). Note that without the shear effects the resonance frequencies are pushed out to much higher values. This lowest order resonance is likely due to an equivalent A_0 Lamb wave mode for which both sides of the shell vibrate in phase.

TABLE I. Elastic and acoustic material properties used in modeling the elastic spherical shell and skull.

	Density (kg/m^3)	Sound speed (m/s)	
		Long	Shear
Air	1.2	333.7	n/a
Skin	998	1496	n/a
Bone	1490	2522.4	1215
Soft tissue	998	1496	n/a

For sound waves coupled to the skull through the air background the enegy which is not reflected, will be diffracted around and induce vibrations within the skull structure. Some of the energy will also penetrate into the cavity resulting in standing wave vibrations but this effect is less significant. An explanation of the interaction between the diffracted acoustic signal and structural vibrations of a fluid-loaded elastic spherical shell is given by Gaunaurd.[10] Using the modal plane wave solution and approximating the skull as a sphere, one can conclude that the surface of the skull vibrates due to a relatively slow-moving diffracted wave which travels on the surface and couples energy into the skull as it propagates.

III. NUMERICAL SIMULATION

Due to the tremendous complexity of the human skull, a numerical simulation algorithm was developed in order to better evaluate patterns of bone-conducted sound as it couples to the skull from an air background. The algorithm is based on a finite element implementation of the acoustic pressure wave equation. Thus shear effects are not taken into account but the near-field effects due to diffraction and evanescent waves are. Because there is so little symmetry and so much complexity in the skull a full 3D simulation is required. The finite element mesh was obtained by CT scanning a skull and using the voxels as brick elements in the mesh. This is possible if the mesh is fine enough such that there are at least 50 nodes per wavelength for the highest frequency in the input signal.

Typical scans of cadaver heads can be very noisy. If one looks at the individual pixels of these images there are many different shades of gray level values. The FE algorithm requires distinct pixel values in which each value corresponds to a material type. Crisper, cleaner images were obtained by CT scanning a dry skull. The scan yielded 360 2D slices with each slice being 1 mm thick. The slices were imported into a medical rendering software package known as Amira and soft tissue representing brain fluid and skin were added to digitally sculpt a replica of a human head. Transducers, attached to the mastoid and forehead, were also drawn in. These transducers were used to check the simulation against a head sensitivity mapping study conducted by the Army Research Laboratory (ARL).[12] Earplugs were also added to

(a)

(b)

FIG. 2. (Color online) (a) Cross-sectional slice of 3D skull image showing location of mastoid-mounted transducers. (b) Cross-sectional slice of 3D skull image showing ear canals with earplugs.

simulate the occlusion effect whereby, for some frequencies, sound is trapped in the ear canals when ear protection is in place. The resultant images are in terms of acoustic properties such that the entire brain appears as a homogenous fluid-gel material as shown in Fig. 2.

The space around the skull is simulated in order to account for diffraction and radiation effects. Background slices are added above and below the skull to make a total of about 500 slices. For a 4 kHz input pulse a voxel size of $1\times1\times1$ mm^3 will ensure 50 nodes/wavelength. Mur type absorbing boundary conditions (ABCs) are enforced on the boundary of the mesh. In order for the ABC to be effective the scatterer must be a minimum of two wavelengths from the outer boundary. Typical meshes consists of $500\times500\times500$ or 125 million nodes. If the center frequency of the input signal is reduced to 2 kHz then the area should be downsampled such that all points on the skull remain at least 2 wavelengths away from the radiation boundary.

The efficient implementation of a simulation with 125 million nodes and usually 20 000 time-steps is achieved through the use of High Performance Computing (HPC) or massively parallel machines. These computers are distributed memory machines, otherwise known as clusters, in which each node has its own memory core and the nodes communicate with each other through dedicated cabling. The program is designed so that each compute-node operates on one slice of the mesh. Therefore 500 compute-nodes are required to complete each simulation with each node operating on $500\times500=250\,000$ pixels. The program contains message passing interface (MPI) directives in order that the pressure information at each slice can be passed to the adjacent slices at every time-step. The program can store the pressure at each pixel for every time slice. The program was benchmarked against analytic and experimental results for a fluid-filled sphere.

In order to demonstrate the effects of scatterer shape, and input angle, on the diffraction pattern and level of acoustic penetration within the scattering object, results in the form of intensity plots are shown in Figs. 3 and 4 for a 2 kHz signal impacting an ellipsoidal shell. Note that an ellipsoid was chosen as it is relatively simple but, more than a sphere, resembles the shape of a typical skull. The ellipsoid is 20 cm long (front to back) 16 cm wide (left to right) and 25 cm high (top to bottom). Shown in Fig. 3 are "snapshot" intensity plots for both the total and the scattered pressure wave. The scattered pressure wave is obtained by subtracting the incident from the total. Figure 4 contains the plots for a wave impacting the ellipsoid on the side. Note that the intensity plots of Figs. 3 and 4 were recorded at 2 mS whereby the incident wave reaches point D at around 0.8 mS. The sound speed for waves traveling on the surface and for those propagating into the interior are calculated from the travel time and dB level drops between point D and points A, B, C. Results are given in Table II.

These results indicate that the majority of the acoustic energy remains on the surface and becomes part of a diffracted wave traveling along the surface. The sound speed of this surface wave depends on the object shape as well as the material properties on either side of the interface. Calculation of sound speeds, based on an acoustic signal traveling from the front to the back and between the front and the side of the ellipsoid, are between 400–500 m/s which are similar to those found experimentally by Stenfelt[1] for speeds found from phase shifts between the mastoids.

The model has also been validated through simulations of the occlusion effect whereby bone-conducted sound can be elevated in ear canals which have been blocked or occluded. Simulations of an acoustic sound field interacting with the human head are shown in Fig. 5(a) for a plane wave hitting the skull and in Fig. 5(b) for a signal coupled through the skull via a mastoid mounted transducer. In both cases the ear canals are occluded in order to demonstrate the occlusion effect whereby sound of certain frequencies is trapped in plugged ear canals. Shown in Table III are the simulated measurements of the pressure in the ear canal, relative to the input signal, for the occluded and unoccluded ear. These results agree with experimental data[13] indicating that the occlusion effect is frequency dependent with a notch between 1 and 4 kHz.

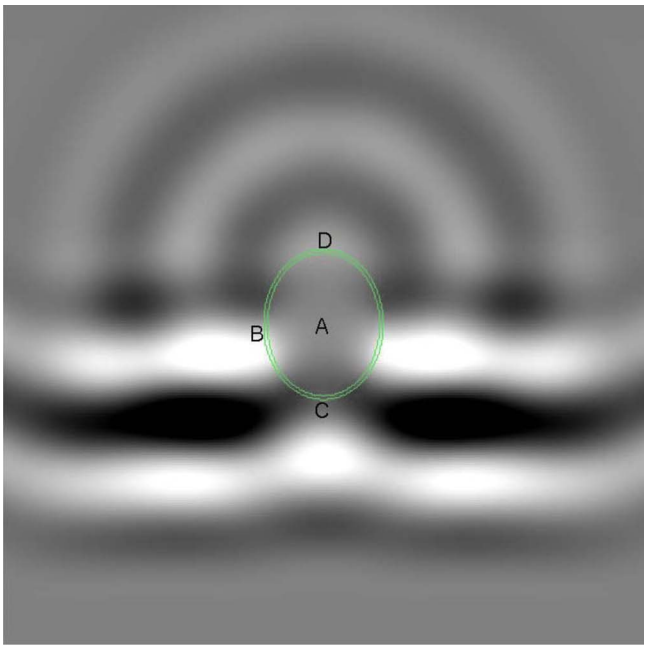

(a)

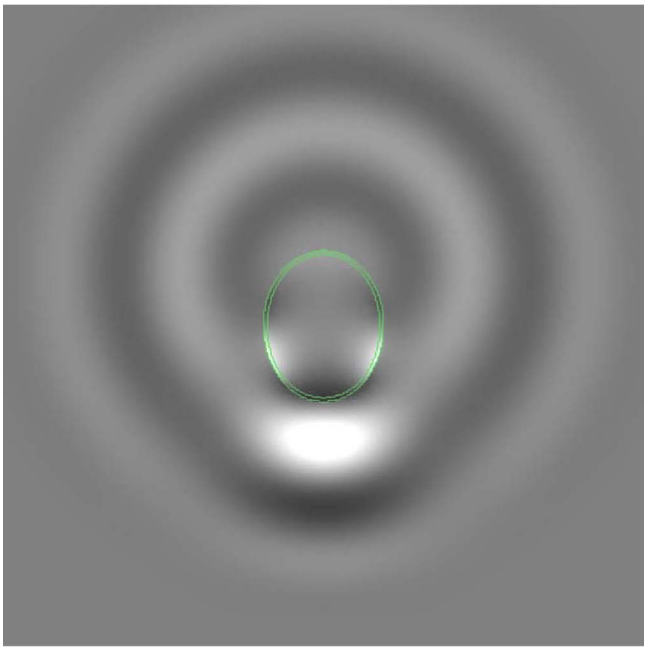

(b)

FIG. 3. (Color online) (a) Pressure intensity plots of a 2 kHz pulsed plane wave propagating through a thin fluid-filled ellipsoid shell. Shell has properties of bone (sound speed and density), fluid has acoustic properties of water. Total sound field. (b) Pressure intensity plots of a 2 kHz pulsed plane wave propagating through a thin fluid-filled ellipsoid shell. Shell has properties of bone (sound speed and density), fluid has acoustic properties of water. Scattered sound field.

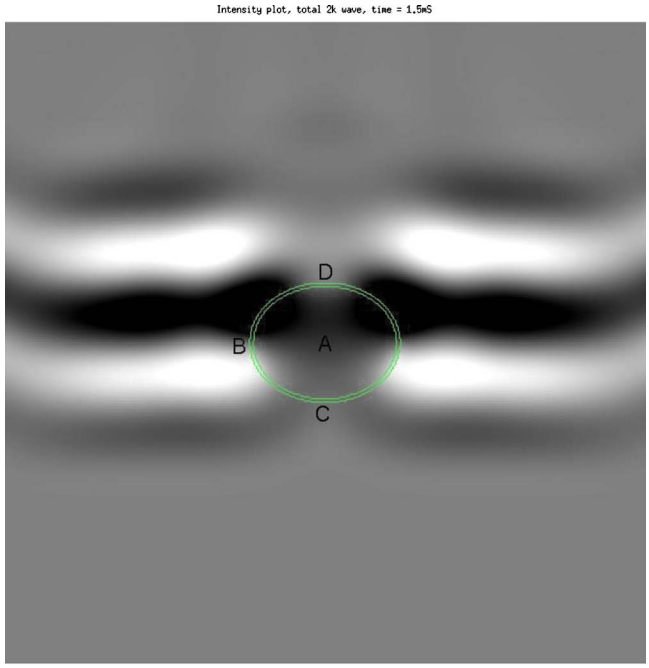

(a)

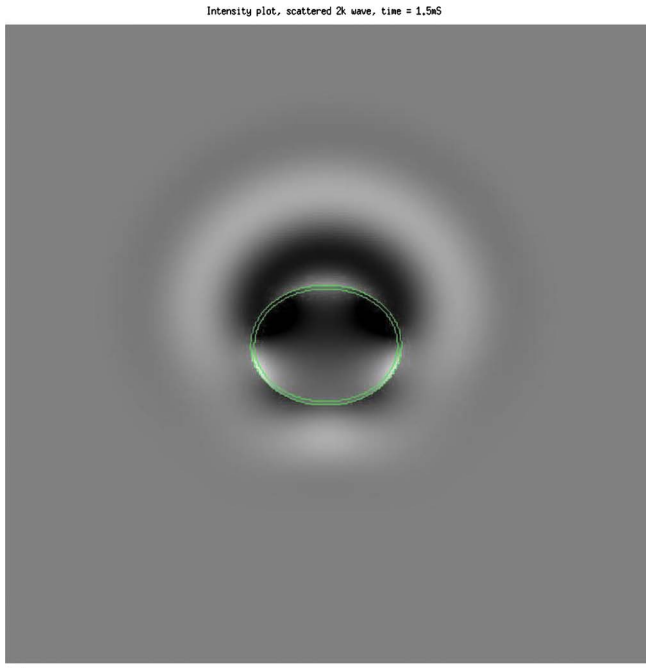

(b)

FIG. 4. (Color online) (a) Pressure intensity plots of a 2 kHz pulsed plane wave propagating through a thin fluid-filled ellipsoid shell. Shell has acoustic properties of bone, fluid has acoustic properties of water. Total sound field. (b) Pressure intensity plots of a 2 kHz pulsed plane wave propagating through a thin fluid-filled ellipsoid shell. Shell has acoustic properties of bone, fluid has acoustic properties of water. Scattered sound field.

IV. CONCLUSION

Both analytic and numerical models are used to evaluate how acoustic energy is converted into bone-conducted sound. Results indicate that most of the sound energy which impinges upon the skull from an outside source is channeled into surface waves on the outside of the skull. The nature of these waves have a complicated dependency on the impedance mismatch at the interface between the air background and the solid bone. Generally these waves, whether they exist mostly in the solid bone or the background medium of air, will travel at much slower speeds than the longitudinal sound speed for bone. The wavelength for these waves is therefore smaller than the wavelength of an acoustic signal which exists solely in bone or in the cranial cavity. Frequencies, at which an integer number plus one-half of surface wave wavelengths fit around the circumference of the sphere,

TABLE II. Comparison of pressure signals for plane wave hitting ellipsoids from the front and side.

	Pressure level (dB)			Equivalent sound speed (m/s)		
Simulation	D→B	D→A	D→C	D→B	D→A	D→C
Front ellipse	−2.6	−16	−4	468	1038	391
Side ellipse	−2.7	−9.3	−3.5	565	1049	415

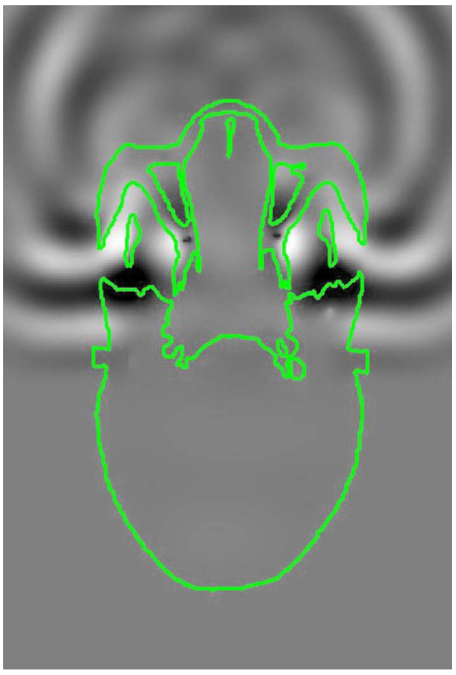

(a)

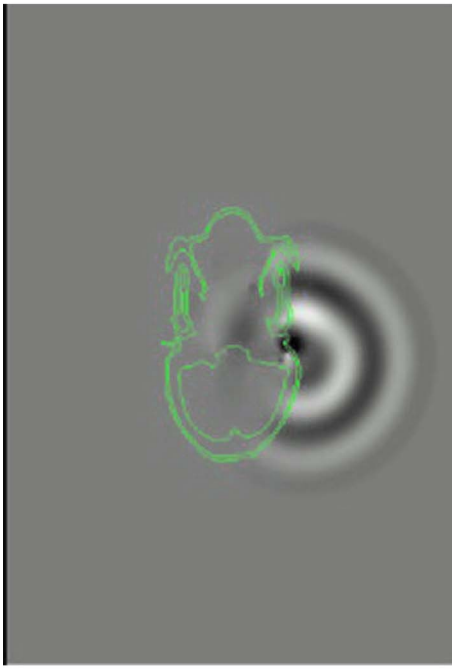

(b)

FIG. 5. (Color online) (a) Pressure intensity plots of acoustic pressure signals as they interact with the head model of Fig. 2. 8 kHz plane wave hitting front of skull. (b) Pressure intensity plots of acoustic pressure signals as they interact with the head model of Fig. 2. 4 kHz mastoid mounted transducer.

TABLE III. Comparison of pressure levels in the ear canal for occluded and unoccluded ear versus frequency.

	1 kHz	2 kHz	3 kHz	4 kHz
Unoccluded ear	−19 dB	−19 dB	−24 dB	−22 dB
Occluded ear	−9.5 dB	−11 dB	−15 dB	5 dB

cause resonant vibrations. The added one-half is due to phase matching the surface wave at the poles of the sphere.

The implications of relatively slow sound and short wavelengths are that resonance frequencies for the skull are lower than if the acoustic energy were confined to standing waves within the cranial cavity wherein the wavelengths are longer. At the acoustic frequencies skull vibrations are analogous to the lowest order flexural modes of a fluid loaded elastic sphere. Of course, the human skull has an intricate structural formation which requires a numerical simulation in order to evaluate a detailed frequency response. Initial numerical models strongly suggest that bone–conducted sounds are confined to the skull surface with wave speeds much lower than the measured speed of sound for boney or soft tissue.

ACKNOWLEDGMENTS

The authors would like to thank the Air Force Office of Sponsored Research for their generous support of this work through Grant No. FA9550-07-C-0084. The authors also acknowledge the support of the Texas Advanced Computing Center (TACC) and the Teragrid network of HPCs for their support of this project. The authors are grateful for the helpful comments of the reviewers.

[1]S. Stenfelt and R. Goode, "Transmission properties of bone conducted sound: Measurements in cadaver heads," J. Acoust. Soc. Am. **118**, 2373 (1994).
[2]B. Håkansson, A. Brandt, and P. Carlsson, "Resonance frequencies of the human skull *in vivo*," J. Acoust. Soc. Am. **95**, 1474–1481 (1994).
[3]G. von Békésy, *Experiments in Hearing* (McGraw–Hill, Oxford, England, 1960), pp 142–150.
[4]F. J. Fry and J. E. Barger, "Acoustical properties of the human skull," J. Acoust. Soc. Am. **63**, 1576–1590 (1978).
[5]D. T. Reilly and A. H. Burstein, "The elastic and ultimate properties of compact bone tissue," J. Biomech. **8**, 393–405 (1975).
[6]P. Uginčius and H. Überall, "Creeping-wave analysis of acoustic scattering by elastic cylindrical shells," J. Acoust. Soc. Am. **43**, 1025–1035 (1968).
[7]H. Überall, L. R. Dragonette, and L. Flax, "Relation between creeping waves and normal modes of vibration of a curved body," J. Acoust. Soc. Am. **61**, 711–715 (1977).
[8]L. Flax, G. Gaunaurd, and H. Überall, "Theory of resonance scattering," in *Physical Acoustics*, edited by W. P. Mason and R. N. Thurston, (Academic, New York, 1981), **15**, pp. 191–294.
[9]J. J. Faran, Jr., "Sound scattering by solid cylinders and spheres," J. Acoust. Soc. Am. **23**, 405–418 (1951).
[10]G. C. Gaunaurd and M. F. Werby, "Lamb and creeping waves around submerged spherical shells resonantly excited by sound scattering," J. Acoust. Soc. Am. **82**, 2021–2033 (1987).
[11]J. McNew, R. Lavarello, and W. D. O'Brien, Jr., "Sound scattering from two concentric fluid spheres," J. Acoust. Soc. Am. **125**, 1–4 (2009).
[12]M. McBride, T. R. Letowski, and P. K. Tran, "Bone conduction head sensitivity mapping: Bone vibrator," Army Research Laboratory, Report No. ARL-TR-3556, 2005.
[13]S. Stenfelt and R. L. Goode, "Bone-conducted sound: Physiological and clinical aspects," Otol. Neurotol. **26**, 1245–1261 (2005).